Backbone Dynamics of the RNase H Domain of HIV-1 Reverse Transcriptase

Geoffrey A. Mueller,‡ Koteppa Pari,‡ Eugene F. DeRose, Thomas W. Kirby, and Robert E. London*

Laboratory of Structural Biology, NIEHS, National Institutes of Health, P.O. Box 12233, Research Triangle Park, North Carolina 27709

Received March 5, 2004; Revised Manuscript Received May 5, 2004

ABSTRACT: Previous NMR relaxation studies of the isolated RNase H domain of HIV-1 reverse transcriptase at low pH have revealed that it is substantially more dynamic and less ordered than the relatively stable and catalytically active *E. coli* RNase HI. Using more recently developed techniques, we have investigated the dynamic behavior of the RNase H domain of HIV-1 reverse transcriptase at a more physiological pH (6.8), under a variety of solution conditions: no Mg^{2+}, 80 mM Mg^{2+}, and 80 mM Mg^{2+} plus AMP ligand. In addition, we have repeated the previous measurements on a sample containing 100 mM sodium acetate, pH 5.4. Under all conditions studied, the order parameters from NMR relaxation analysis are uniformly high (>0.8) for most of the domain with the exception of the C-terminal region. Subtle differences can be found among the conditions studied, although the statistical significance of the differences is marginal. Residues 71−114 show a slight increase in order parameter with the addition of 5′-AMP. Conformational exchange, measured with CPMG relaxation dispersion experiments in the presence of Mg and AMP, were detected for some NH sites, predominantly located in the N-terminal region of the protein near strands β2 and β3 and helix α_A (residues 28−69). In contrast with earlier studies indicating pathologically extreme dynamic behavior that apparently correlated with inactivity of the isolated domain, the relaxation analysis under the conditions of the present study yielded parameters that are more similar to those of the active *E. coli* RNase HI. A comparison of the order parameters obtained from a model-free analysis of the relaxation data with the B-factors in the crystal structures of the RNase H domain, both for the isolated domain and for the full HIV-1 reverse transcriptase structure, suggests that the dynamic behavior is similar in all cases.

The human immunodeficiency virus (HIV) is a retrovirus, which requires the reverse transcription of viral genomic RNA into DNA (*1*−*3*). This process is catalyzed by a bifunctional enzyme, HIV reverse transcriptase (RT),[1] which consists of two subunits, p51 and p66. Both subunits contain a DNA polymerase domain, while p66 contains an additional ribonuclease H domain (RNase H). The RNase H domain performs two functions. It degrades the RNA template and specifically removes the RNA primer from the RNA/DNA hybrid. The domain can be isolated and expressed as a stable protein, which is either inactive (*4, 5*) or very weakly active (*6, 7*).

The basis for the inactivity of the isolated RNase H domain of RT has been the object of many studies and considerable speculation. It has been suggested that inactivity of the isolated domain could result from the absence of critical binding residues present in the full RT structure (*8*) or from structural and/or dynamic differences between the isolated RNase H domain and the RT-incorporated RNase H domain. A very substantial case can be made for the first explanation given above. For example, construction of a chimeric RNase H domain that contained the additional structural elements from the *E. coli* RNase HI (residues 76−102) resulted in a hybrid enzyme with ∼10-fold greater nucleolytic activity than the full RT (*9*). Restoration of activity to the isolated RNase H domain also has been achieved by the addition of a His-tag to either the N- or C-terminal positions, although the nucleolytic activity of the resulting constructs was lower than that of the full RT enzyme (*7*). Since both the His-tag and the additional loop are basic in nature, it has been suggested that the activity observed for these constructs could result from enhanced binding of the nucleic acid substrate.

A second proposed explanation for the inactivity of the isolated RNase H domain of RT is that its structure differs significantly from that adopted in the full RT molecule. However, comparisons of the crystal structures of this domain in isolation or in intact RT do not appear to indicate any major differences (*8, 10*). A recently determined solution structure also shows homology to the crystal structure of the isolated domain, with the exception of the C-terminal helix, for which the corresponding resonances are strongly exchange broadened (*10*). A more complete analysis of the ensemble of crystal structures for RT indicates that this helix is also frequently absent in the crystalline state, leading to the conclusion that even in the full RT molecule, this structural element has marginal stability (*10*). Recent studies of the histidine-containing active site loop, which is adjacent in sequence to the C-terminal helix in the RNase H domain,

* Corresponding author. Phone 919-541-4879. Fax: 919-541-5707. E-mail: london@niehs.nih.gov.

‡ G.A.M. and K.P. contributed equally to this paper.

[1] Abbreviations: HIV-1, human immunodeficiency virus type 1; RNase H domain, the ribonuclease H domain of HIV reverse transcriptase; RT, reverse transcriptase; NOE, nuclease Overhauser enhancement; CPMG, Carr, Purcell, Meiboom, and Gill; AMP, 5′-adenosine monophosphate.

10.1021/bi049555n
Published on Web 06/30/2004

also were interpreted to indicate that this region of the isolated domain remains structured (*11*).

A third proposal for the inactivity of the isolated RNase H domain of HIV-1 RT is based on the previous conclusion that its intramolecular dynamic behavior is so extreme that it results in inactivity. In addition to the exchange broadening noted above for the C-terminal helix, NMR relaxation data obtained for the isolated RNase H have indicated that the isolated domain is characterized by extensive internal mobility throughout its structure (*12*). In this study, a substantial fraction (35%) of the order parameters derived using a Lipari−Szabo analysis were <0.7 (*12*, *13*). In addition to the C-terminal residues, the loop regions between β-strands β_1 and β_2 and between α-helix α_B and β_4 were identified as particularly mobile regions of the protein (*12*). A comparison of the dynamic behavior of the RT RNase H domain with that of the *E. coli* RNase HI led to the proposal that loss of structure and concomitant increase in residue mobility is a critical determinant of the loss of catalytic activity of the isolated RNase H domain (*14*). It was further concluded that since the dynamic differences between the two enzymes are not localized to the C-terminal region, the loss of activity correlated more significantly with the overall increase in dynamic behavior and the apparent instability of the entire isolated RNase H domain.

The previous dynamic characterization of the HIV-1 RNase H domain was clearly a significant contribution to the literature. However, since the previously reported studies, several important developments in methodology for protein relaxation measurements have occurred such as the introduction of relaxation-compensated CPMG sequences used to measure T_2 and relaxation dispersion (*15*). Probably the most important development is the introduction of pulse sequences for relaxation data acquisition that avoid saturating the water resonance (*16*−*18*). This problem had been appreciated for some time and is presumably the reason that the previous study was performed at low pH (5.4), at which the exchange rate of labile amide protons is reduced. In terms of analysis, model selection for Lipari−Szabo "model-free" analysis continues to improve from the Mandel et al. protocol introduced in 1994 to the Akaike Information Criteria (AIC) of d'Auvergne and Gooley in 2003 (*13, 14, 19*). In light of numerous new developments and our observation that Mg strongly affects the HSQC spectra (*10*), it seemed appropriate to reinvestigate the relaxation characterization of the RNase H domain under the previous conditions as well as some more physiologically relevant ones.

As noted above, we have recently performed NMR measurements on the isolated RNase H domain of HIV-1 RT at neutral pH in the presence of high Mg^{2+} concentrations and found the domain to be sufficiently well behaved to allow a structural determination for all but the C-terminal region (*10*). To fully evaluate previous proposals regarding the relationship of internal dynamics with enzyme activity, we now have performed a relaxation analysis of the dynamic behavior of this domain at neutral pH (6.8), in an "apo-state" with no salts, in the presence of Mg^{2+}, and in the presence of Mg^{2+} plus AMP. AMP and other mono- and dinucleotides have been reported to be weak inhibitors of the RNase H activity of HIV-1 RT (*20, 21*). Interestingly, Chattopadhyay et al. reported improved crystal growth when the RNase H domain was incubated with Mg^{2+} and AMP (*22*). The studies described here provide further insight into the behavior of this essential enzymatic activity in the life cycle of HIV.

MATERIALS AND METHODS

NMR Methods. The sample preparation was exactly as described previously (*10*). Four different solution conditions were studied. They are referred to as: "low pH", "Apo", "Mg", and "Mg plus AMP". All solutions contain 0.05−0.1 mM AEBSF, 50 μM DSS, and 10% ^2H_2O. The low-pH buffer, consisting of 100 mM sodium acetate-d_3, pH 5.4, is intended to mimic the previous studies. The other buffers contain zero (Apo) or 80 mM $MgCl_2$ (Mg), 10 mM Tris-d_{11}, pH 6.8. In some studies, 20 mM 5′-AMP (Mg plus AMP) was also added to the Mg sample. The numbering of the amino acid residues in the protein is 1−138, which includes four N-terminal residues (MNEL) followed by residues 427−560 of the HXB2 strain of HIV-1. Hence, adding 422 to the residue number in the current study gives the corresponding residue in the p66 subunit of HIV-1 RT for strain HXB2. The numbering used facilitates comparisons with previous NMR studies (*12*, *23*, *24*). A uniformly labeled [^{15}N, ^{13}C]-RNase H sample was used for backbone and side chain assignment, as well as relaxation experiments (T_1, T_2, and NOE). The RNase H samples used in the relaxation dispersion experiments were uniformly ^{15}N labeled. The concentration of the protein was initially 1.0 mM, and upon addition of $MgCl_2$ and AMP it was approximately 0.8 mM. A series of HSQC spectra obtained at different concentrations showed a linear dependence of intensity on concentration from 0.5 to 1mM and was only slightly nonlinear out to 1.5 mM, indicating minimal aggregation at the concentrations used for relaxation measurements (data not shown).

The NMR spectra of the RNase H domain in the various buffers were assigned in separate studies. The assignments in 100 mM sodium acetate pH 5.4 were taken from the BRMB as assigned by Powers et al. (*24*). The shifts therein were referenced to TSP as opposed to DSS in our sample; therefore, the resonances generally differed by a constant offset but could be readily identified. Compared to the previous 107 peaks that were analyzed, we confidently assigned 98 that had no significant overlap. The HSQC spectra of the sample with 80 mM $MgCl_2$ was assigned previously with standard triple-resonance techniques (*10*). The assignments of the HSQC spectrum for the apo-state were made by following the titration from 0 to 80 mM $MgCl_2$ (*10*). The assignments for the Mg + AMP spectrum were made using standard triple-resonance techniques and will be reported elsewhere.

The relaxation data were acquired at 11.7, 14.1, and 18.8 T on Varian INOVA spectrometers. The T_1, T_2, and NOE data were acquired according to Farrow et al. at 11.7 and/or 14.1 T (*18*). The relaxation dispersion data were acquired according to Mulder et al. (*25*), as indicated. The spectra were processed with NMRPipe and analyzed with NMRVIEW on LINUX (Red Hat 7.2) and Macintosh (OS X 10.2) workstations (*26, 27*). Experimental uncertainties in the R_1 and R_2 measurements were calculated from Monte Carlo-simulated estimates using the standard deviation of the noise (*28*). The error in the NOE experiment was calculated as the standard deviation in the noise divided by the intensity of the peak in the reference spectrum. The relaxation analysis

module of NMRVIEW 5.0.4 was corrected to properly output errors as posted on our website (http://dir.niehs.nih.gov/dirnmr). The value for rotational correlation time was calculated from the trimmed-mean of R_2/R_1 using the software QUADRIC 1.11 (*29, 30*). The fits of the T_1, T_2, and NOE data to model-free equations were performed with Modelfree 4.15. For the purpose of fitting the data, the errors were assigned according to the fit, but the minimum error was set to 4%. The value used for ^{15}N CSA was −170 ppm and the N−H bond length was 1.02 Å.

The relaxation data were fit to the five motional models described by Mandel et al. (*13, 14*). The purpose of the fitting procedure is to select from among five dynamic descriptions for the nuclei that correspond to: (1) internal motion so rapid that its only effect is to reduce the order parameter from 1 to S^2; (2) fast internal motion that produces a significant spectral density and hence contributes significantly to the observed relaxation; (3) a slow (μs to ms) component of motion that results in exchange broadening and consequent contribution to the transverse relaxation rate; (4) a combination of models 2 and 3 in which both τ_f (fast-time-scale motion) and R_{ex} (rate of chemical exchange) contribute to the observed relaxation; (5) two components of internal motion corresponding to $\tau_f < 100-200$ ps and a slower component characterized by τ_s with $\tau_f < \tau_s < \tau_c$, and consequently two independent order parameters for the different types of internal motion: S^2, S_f^2, and $S_s^2 = S^2/S_f^2$. Model selection was based on Akaike's Information Criteria (AIC), which bases the selection on the minimum AIC defined by:

$$AIC = \chi^2 + 2k \quad (1)$$

where χ^2 is defined according to [2] and k is the number of model-free parameters in the motional model (*19*). This approach biases the analysis toward models that require fewer adjustable parameters and is superior to previous statistical methods in balancing under- versus over-fitting the number of parameters (*19*). The error in the fit is given by

$$\chi^2 = \sum_{i=1}^{N}\sum_{j=1}^{M}\left\{\frac{(R_{1ij} - \hat{R}_{1ij})^2}{\sigma^2_{R_1ij}} + \frac{(R_{2ij} - \hat{R}_{2ij})^2}{\sigma^2_{R_2ij}} + \frac{(\mathrm{NOE}_{ij} - \hat{\mathrm{NOE}}_{ij})^2}{\sigma^2_{\mathrm{NOE}ij}}\right\} \quad (2)$$

in which R_{1ij}, R_{2ij}, and NOE_{ij} are the measured values and $\hat{R}_{1ij}$, $\hat{R}_{2ij}$, and $\hat{\mathrm{NOE}}_{1ij}$ are the fitted values for ith spin and the jth static field (*14*). The corresponding experimental uncertainties are given by σ_{R_1ij}, σ_{R_2ij}, and $\sigma_{\mathrm{NOE}ij}$.

The relaxation dispersion data used the output intensities from NMRVIEW and were analyzed with MATLAB scripts to fit the equations given by Tollinger et al. (*31*).

B-Factor Comparisons. The B-factors for the RNase H domain were analyzed from six crystal structures, four from the p66 subunit of RT [1RT7 (*32*), 1RTD (*33*), 1RTH (*34*), and 1C9R (*35*)] and two from the isolated domain [1HRH (*8*) and 1RDH (*22*)]. Further, the structures 1C9R and 1RTD belong to the p66/p51 in complex with double-stranded DNA. Since the NMR analysis concerned ^{15}N dynamics, it seemed appropriate to use the B-factor from the backbone nitrogen of each residue, where available. In the case of 1RDH, only the Cα coordinates were available, so the B-factors for the Cα were used. The four p66 subunits of RT had very similar mean B-factors over all residues. With respect to the above list they were 50 ± 15, 52 ± 15, 58 ± 29, and 51 ± 30. The p66 structures include 2 from the $P2_12_12_1$ space group (1RT7 and 1RTH) where the C-terminal helix is not observed and two where it is observed (1C9R and 1RTD). Note that 1RTD had two molecules in the asymmetric unit, so up to five data points could be used for averaging the B-factors of p66. In cases where data were missing, e.g., the C-terminal helix, only the available data points were used. For the isolated RNase H, domain there were two molecules in the asymmetric unit in both cases, so up to four data points were used to calculate the average B-factor where data were available. The isolated domains also had similar overall mean B-factors, with subtle differences between the molecules in the asymmetric unit: 1HRH-A 36 ± 12, 1HRH-B 36 ± 11, 1RDH-A 29 ± 11, 1RDH-B 28 ± 10.

Order Parameter Predictions. The prediction of fast-time-scale order parameters from crystal structures was calculated using the program of Zhang and Brushweiler (*36*). The program predicts order parameters based on a contact model and is based on empirical observations of previously measured order parameters and corresponding crystal structures. The RT structure used was 1RT7. Hydrogen atoms were added and side-chains completed where necessary using CNS (*37*).

RESULTS

Fast-Time-Scale Dynamics. The dynamic behavior of the RNase H domain on a time scale of nanoseconds to picoseconds was assessed by measuring ^{15}N R_1, R_2, and steady state ^{15}N{^{1}H} NOE relaxation parameters at 11.7 and 14.1 T. The R_1, R_2, and NOE data at 14.1 T obtained under all solution conditions are presented in Figure 1. Following the discussion given by Davies et al., we have labeled the helices α_A, α_B, α_D, and α_E, since the helix corresponding to α_C in *E. coli* RNase H is not present in the HIV RT RNase H domain (*8*). Addition of Mg^{2+} ions results in many significant shifts of the amide resonances, greatly improving the dispersion of the ^{1}H−^{15}N HSQC spectrum (*10*). Some of the most congested regions of the spectrum, corresponding to shifts near the random coil values, show particular improvement. The overlap in the apo state is significant, so that at 11.7 T we are only confident of 59 amide resonances that are sufficiently well-resolved to allow accurate relaxation measurements. The increased signal-to-noise and dispersion at 14.1 T allows us to report measurements on 83 amide resonances. Similarly, we found that the low-pH sample had 98 resolvable resonances at 14.1 T. As shown in Figure 1, several of the loop regions are relatively mobile, with elevated R_1, and lower R_2 and NOE ratios. In particular, the region between β_4 and α_B, the region between α_B and α_D, and the N- and C-terminal regions of the protein appear to be highly dynamic. In the full RT structure, the loop between α_B and α_D makes contact with other residues in the p66 subunit, so that the enhanced mobility for these residues may result from the elimination of the interactions with other residues in the p66 subunit. Elevated R_2 values were also measured for residues at both ends of helix α_E, probably resulting from conformational exchange. Overall, the relaxation behavior under all conditions appears to be very similar.

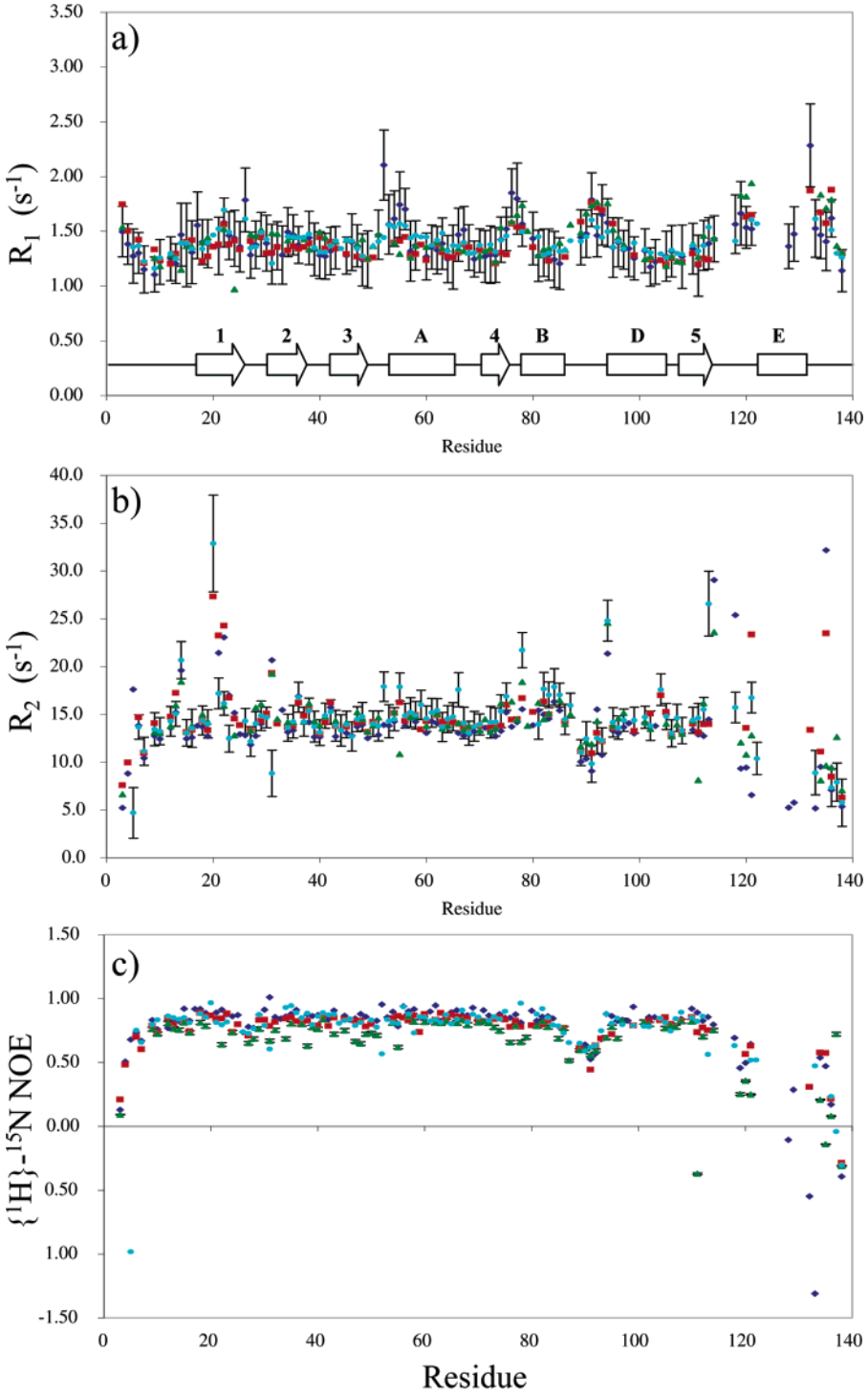

FIGURE 1: Measured relaxation parameters at 14.1 T. Presented are the R_1 (a), R_2 (b), and {^{1}H}−^{15}N NOE (c) for RNase H in the low-pH (cyan circles), apo (green triangles), Mg (red squares), and Mg plus AMP (blue diamonds) buffers measured at 14.1 T. Error estimates were similar for all fitted measurements but for clarity are displayed only for one set of data. The errors displayed are from (a) AMP, (b) low-pH, and (c) apo solutions.

At neutral pH, there appears to be a slight increase in the average NOE going from apo (0.67 ± 0.24) to Mg (0.76 ± 0.28) or Mg plus AMP conditions (0.76 ± 0.29). Nevertheless, the overall appearance of the relaxation data from the N-terminal residue to the end of strand β_5 is characteristic of a well-folded protein.

In addition to the loops noted above, a number of residues in β-strands 1−3 were characterized by elevated R_2 values, particularly in the presence of Mg and Mg plus AMP. These three strands make up the antiparallel half of the core β-sheet and pack against the C-terminal helix α_E, which is known to be dynamic. Presumably, motion of the C-terminal helix could produce a time-dependent variation in the magnetic environment of these residues, resulting in exchange broadening. Finally, Asp21, which is located in the middle of the strand β1, as well as some nearby residues, exhibit highly elevated R_2 values. Since this is the only residue involved in binding both divalent metal ions observed in the crystal structure (*8*), this broadening probably results from the exchange of the Mg^{2+} ions and any associated conformational

rearrangements related to ion binding. On the basis of the K_D values previously determined, at 80 mM Mg^{2+}, metal site A is fully occupied, while site B is ~68% occupied. The elevated R_2 values are not found in the apo state, supporting the notion that Mg^{2+} binding is the cause of this result.

To analyze the data with the model-free formalism (*13*), we first considered motional anisotropy of the protein diffusion, which can interfere with the mobility analysis of the individual residues. In the crystal structure of the isolated RNase H domain, 1HRH (*8*), the principal moments of inertia have normalized ratios of 1.8:1.4:1, indicating the possible significance of motional anisotropy. To account for possible anisotropic diffusion, the T_1/T_2 data were fit to a model that allowed isotropic, axially symmetric, or fully asymmetric diffusion (*29*). The principal axes of the diffusion tensor determined in this way for the protein under all solution conditions were within a few degrees of the inertia tensor (data not shown) determined from the 1HRH structure. The rotational correlation time (τ_c) was initially estimated from the trimmed-mean of T_1/T_2 data (*29*, *30*). In the case of the Mg plus AMP solution, the fit to an isotropic diffusion model compared with the fit using an axially symmetric diffusion tensor yielded a marginally reduced χ^2: the *F*-test for the apo state was 5.3, and the *F*-test for Mg + AMP was 3.6. However, in the case of the Mg only buffer, the data fit significantly better to the axially symmetric diffusion model (*F*-test = 11.7), but there was no further improvement when fitting to a fully asymmetric diffusion tensor (*F*-test = 1.1). For the axially symmetric model, the ratio of the diffusion rates about the parallel vs perpendicular axes ($D_{parallel}/D_{perpendicular}$) of 1.2 is near 1.0, so that the deviation from isotropic motion is small. This probably results from the contributions of the hydration sphere as well as the partially disordered C-terminal region of the protein.

Several different subsets of the relaxation data measured at 11.7 and 14.1 T were fit with the model-free formalism in order to assess the validity of the data and the sensitivity of the conclusions to the various measurements for all three solution conditions. Specifically, the model-free analysis was applied using three different sets of data: (1) data only acquired at 14.1 T, (2) T_1 and NOE data acquired at both fields but only T_2 data at either field, or (3) using only T_1 and NOE data and fitting the original Lipari−Szabo equation (model 2) (*13*). The order parameters determined did not vary significantly using any of the subsets of data described above. The individual residue variations were usually on the order of a few percent. Selection from among the five model-free "models" also showed a limited dependence on the above data fitting options. At most, model selection changed for 10−15% of the residues, dependent on the data subset used, but the order parameters did not change significantly. In addition, all of the above data were fit using an axially symmetric diffusion model, even if the previous tests indicated that it might not provide a significantly better description of the motion. This is consistent with value of $D_{parallel}/D_{perpendicular}$ close to 1.0. The correlation coefficients of S^2 for different data input are typically greater than 0.9. In summary, neither the diffusion model nor the inclusion of different data subsets strongly affected the results.

The order parameters reported in Figure 2 reflect what we consider to be the most reasonable fits and assume isotropic diffusion in all cases. For the Mg and Mg plus AMP conditions, we report the fit using R_1 and NOE data obtained at 11.7 and 14.1 T and R_2 at 11.7 T only (*38*). Using R_2 data from only one static field obviates the need to assume a field dependence of R_{ex} (*39*). For the low-pH and apo states, we report the S^2 values using only the 14.1 T data as discussed above. As can be seen from Figure 1, the R_1, R_2, and NOE profiles show a qualitatively similar residue number dependence for all solution conditions. After model selection, τ_c was optimized again by fixing the motional model and fitting for the best τ_c. Only residues that met the Modelfree program criteria for a "good" fit based on Monte Carlo-simulated error distributions were used for the refit τ_c (*14*). The τ_c values were 9.8 ns for the low-pH sample, 9.7 ns for the apo protein, 9.6 ns for the Mg only sample, and 9.7 ns for the sample containing Mg plus AMP. After this iterative procedure, the rotational correlation time was fixed and the data fit again to the motional models for selection and determination of final values.

Table 1 summarizes the model selection, and Figure 2 shows various plots of S^2. A more detailed tabulation of the fitted parameters is provided in Supporting Information. As is apparent from Figure 2a, the dynamic descriptions of the RNase H domain at neutral pH are very similar. A close inspection of Table 1 reveals that there is a relatively greater requirement for models 3 and 4 for the sample containing Mg only, indicating a greater requirement for "slow" dynamic behavior, characterized by τ_{ex}, constrained by the relation: $\tau_f < \tau_c < \tau_{ex}$. A comparison of the order parameters reported previously for the RT RNase H domain measured at low pH (Figure 2b) with the results obtained here indicates significant differences between the two studies performed under nominally identical conditions. Alternatively, the variability of the relaxation data among the four conditions described in the present study is more limited. Additionally, the number of residues with less complicated motional descriptions is similar to that of the catalytically active *E. coli* enzyme, as shown in Table 1.

The plots of S^2 for RNase H under the solution conditions studied here are very similar. The mean and standard deviations for different regions of the protein are shown in Table 2. The overall correlation of the S^2 values from the different solutions is constantly positive. Pearson's *r* is >0.5 for all S^2 comparisons, except for the low-pH versus apo, which is 0.1. Upon inspection, the datasets are actually very similar (see Table 2 and Figure 2), but the narrow range of values exaggerates the differences between the correlation coefficient for the two datasets. The S^2 values for the two samples containing Mg show the greatest similarity, with $r = 0.74$. In all cases, the C-terminal region, with the exception of residues 132 and 134−136, displays significantly lower order parameters than the rest of the domain, as has been observed before (*12*). For these residues, the values of χ^2 are generally higher than those of the other residues, suggesting that none of the dynamic models provides a good description of the motion.

The effects of AMP addition were assessed as a comparison of the S^2 values using eq 3:

$$\Delta S^2 = S^2_{Mg+AMP} - S^2_{Mg} \quad (3)$$

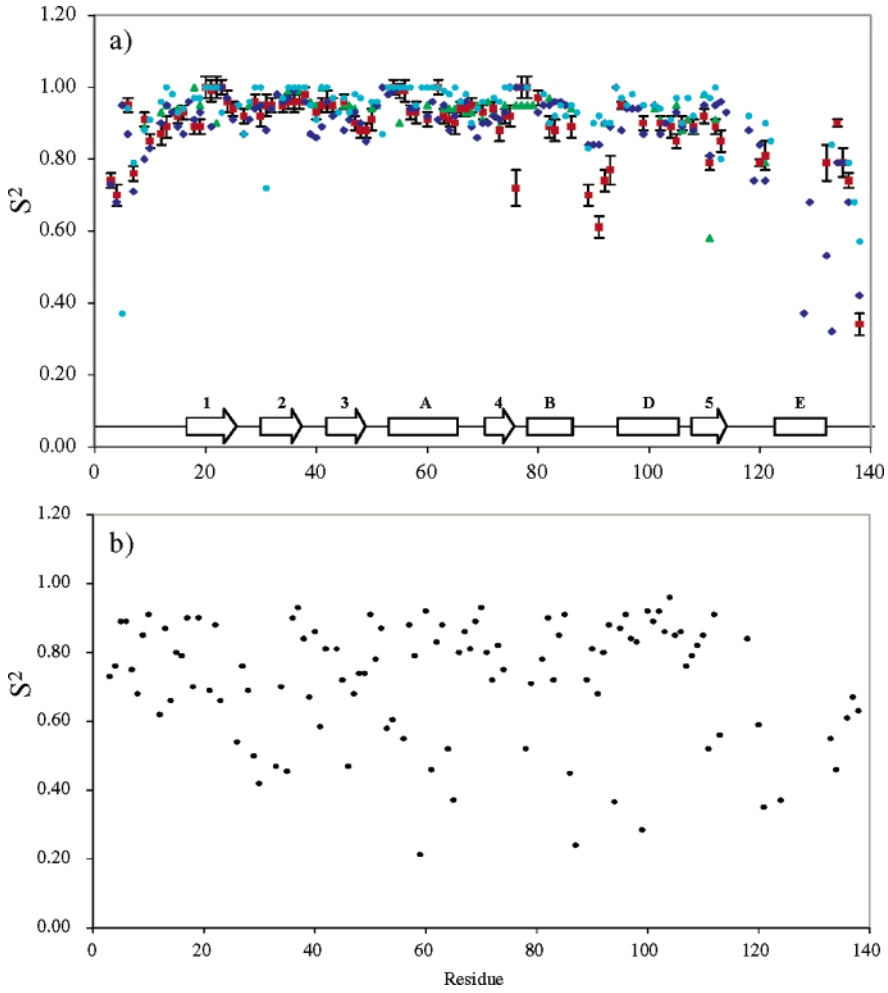

FIGURE 2: Comparison of order parameters under different solution conditions. (a) Order parameters for RNase H determined under different solution conditions: low pH (cyan circles), apo (green triangles), Mg (red squares), and Mg plus AMP (blue diamonds). (b) Order parameters taken from Powers et al. (*12*). The secondary structure is indicated. Error estimates were similar for all four solutions but for clarity are displayed only for the Mg-only sample.

Table 1: Summary of Model Selection[a]

	RNase H domain of HIV-1 RT										*E. coli* RNase HI[c]	
	0 Mg^{2+},[b] 100 mM sodium acetate, pH 5.4		0 Mg^{2+}, 100 mM sodium acetate, pH 5.4		0 Mg^{2+}, pH 6.8		80 mM Mg^{2+}		80 mM Mg^{2+} + 20 mM AMP		0 Mg^{2+}, 100 mM sodium acetate, pH 5.5	
model selected	no. of residues	%	no. of residues	%	no. of residues	%	no. of residues	%	no. of residues	%	no. of residues	%
1	14	13	55	56	25	30	32	40	67	61	67	58
2	7	7	25	26	52	63	16	20	33	30	9	8
3	15	15	13	13	1	1	23	29	4	4	29	25
4	39	36	5	5	5	6	9	11	3	3	2	2
5	32	30	0		0	0	5	6	2	2	9	8

[a] Different motional models for the RNase H domain of HIV-1 RT under different solution conditions are compared with those found for the catalytically active *E. coli* RNase H (*12, 14*). The number of residues that fit to a given motional model and the corresponding percentage requiring each model are indicated. Note that in previous analysis of the relaxation data of the RNase H domain of HIV-1 RT (*12*), six motional models were used. The analysis included an additional model similar to model 4, which included S^2_f, and restricted S^2_s to range from 0.7 to 0.9. In the table, this model is grouped with model 4 because it includes an R_{ex} term. [b] Taken from Powers et al. (*12*). [c] Taken from Mandel et al. (*14*).

By defining ΔS^2 in this way, numbers greater than zero indicate greater order in the presence of AMP. There appears to be a general rise in ΔS^2 beginning approximately after residue 71, which is the beginning of strand β_4 (data not shown). In fact, the average ΔS^2 for residues 1−70 is 0.00 ± 0.04, where the same average for residues 71−114 is 0.09 ± 0.06. These are statistically overlapping distributions, but the trend is apparent (also see Table 2). The correlation coefficient of S^2_{Mg} and S^2_{Mg+AMP} for various regions also confirms this trend. For residues 1−70, Pearson's r equals 0.75; for residues 71−114, r equals 0.38, and for residues 115−138, r equals 0.79. The change in S^2 for residues after number 70 is shown schematically on the structure in Figure 3. We note that heteronuclear NOE data for the apo state also show that residues 1−70 typically have lower NOE values than the other two conditions.

Slow-Time-Scale Dynamics. The slow, μs to ms motions of RNase H were examined using CPMG relaxation disper-

Table 2: Average Order Parameters by Region[a]

	solution conditions			
residues	low pH	apo	Mg	Mg+AMP
all	0.94 ± 0.08	0.93 ± 0.06	0.89 ± 0.10	0.89 ± 0.12
1−70	0.95 ± 0.09	0.94 ± 0.04	0.93 ± 0.06	0.92 ± 0.07
71−114	0.94 ± 0.05	0.92 ± 0.08	0.87 ± 0.09	0.92 ± 0.05
115−138	0.79 ± 0.13	0.79[b]	0.74 ± 0.18	0.65 ± 0.19

[a] Order parameters were averages for different regions of the protein for four different solution conditions as described in the text. [b] $n = 1$.

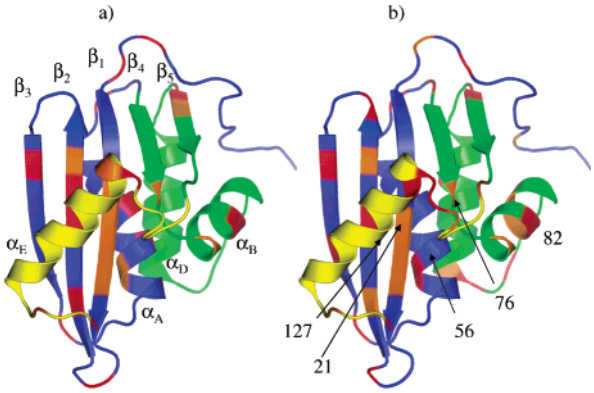

FIGURE 3: Motional subdomains of the RNase H domain of HIV-1 RT. A ribbon diagram model of the RNase H domain based on crystallographic data (*10*) is presented. Residues 1−70 are shown in blue, 71−114 are in green, and 115−138 including the C-terminal helix α_E are colored yellow. Residues 71−114 showed an increased order parameter upon addition of AMP. The secondary structure elements and Mg binding residues 21, 56, 76, and 127 are indicated, as is Gly82, mentioned in the Discussion. Residues that show measurable R_{ex} in the Mg (a) and Mg plus AMP (b) solutions are red, and residues with elevated R_2 values are shown in orange.

sion experiments acquired at 11.7 and 18.8 T for both samples containing Mg and at 14.1 T for the low-pH state (*15*, *25*). The CPMG data were fit according to previously published procedures (*31*). Examples of typical relaxation dispersion data are shown in Figure 4. The plot of resonance intensity versus ν_{CPMG} for Glu92 shown in Figure 4a is typical of 79% of the residues. A second group of 21% of the residues, typified by the plot for Thr48 in Figure 4b, fall into the fast exchange group, for which an R_{ex} value could be extracted from the analysis (Table 3). Statistically, only three fits were significantly improved using the slow exchange equation of Tollinger et al. (*31*), and examination of the spectra eliminated the conclusion that these residues undergo slow chemical exchange. Of course, the most severely exchange-broadened resonances corresponding to residues in the C-terminal helix are not included in the table, since they have not been observed.

The model selection approach appears to indicate that the apo and Mg-AMP samples can be described primarily by models 1 and 2, while the Mg sample shows an increased requirement for models 3 and 4, which include an R_{ex} term. Specific exchange effects can be observed for Asp21 and residues nearby in space. Since Asp21 is involved in binding both of the complexed metal ions in the reported crystal structure (*8*), this suggests that exchange of Mg^{2+} from binding site 2 is slow enough to lead to exchange broadening. Asp21 has one of the broadest ^1H line-widths measured in RNase H (16 Hz versus the mean 12 ± 2 Hz). Also, on the basis of our previous study, site 2 is only partially occupied at 80 mM Mg^{2+}, supporting an exchange contribution (*10*). The CPMG experiments indicate that most of the residues of the RNase H domain do not exhibit detectable slow exchange behavior. In general, the correlation of residues requiring R_{ex} terms obtained from the CPMG analysis relative to that derived from the model-free analysis was found to be marginal. This is likely attributable to two reasons. First, the rates measured are close to the detectable limit ($\tau_{ex} \sim$ ms) for this experiment, so the rates measured are likely to be imprecise. Indeed, the τ_{ex} terms predicted from the model-free analysis are on the order of 1 ms (Supporting Information). The shallow dependence of intensity versus ν_{CPMG} shown in Figure 4a makes the fitting of the parameters very difficult, as discussed by Kempf and Loria (*40*). Second, the CPMG studies depend on the size of the chemical shift difference, $\Delta\omega$, between two states, and this parameter varies widely from residue to residue. In fact, the residues that show slow exchange behavior in the CPMG studies correlate strongly with those that exhibit the largest chemical shift differences upon addition of Mg^{2+} and subsequently AMP.

Despite some inconsistencies, we note the following generalizations. Residues that show detectable slow-motion exchange are located predominantly in the N-terminal half of the protein. In the solution containing Mg^{2+}, 15 residues show detectable exchange and 12 are located in the N-terminal half. In the solution containing Mg^{2+} plus AMP, 21 residues show detectable exchange and 13 are located in the N-terminal half. Although the total number of residues with R_{ex} contributions increases, only nine specific residues show exchange contributions in both solutions. Nevertheless, the clustering of residues exhibiting slow exchange behavior in the N-terminal portion of the protein is probably significant. The residues that exhibit exchange contributions are shown in red on the structures in Figure 3a,b, where 3a shows the Mg-only sample and 3b shows the Mg plus AMP sample. A closer examination of the residues experiencing slow exchange in the core β-sheet revealed that many were likely to interact with the C-terminal helix, α_E. The fact that in the presence of AMP more residues show detectable R_{ex} may be attributed to the conformational exchange of helix α_E. Gly82, which shows detectable R_{ex} and is located in the middle of helix α_B, is also identified in Figure 3. This residue is located next to Ile83, which has been identified as part of the HIV-1 RT primer grip (*41*).

Finally, relaxation dispersion experiments for the amide side chains were performed at 11.7 and 14.1 T (data not shown). In this study, the NH_2 groups were not assigned; however, no NH_2 cross-peaks showed any dependence on the CPMG field strength. Therefore, the NH_2 groups undergo primarily fast-motion dynamics.

DISCUSSION

HIV-1 reverse transcriptase (RT) is characterized by both DNA polymerase and RNase H activities that are localized on separate active sites. The RNase H domain has been isolated and studied by both X-ray crystallography (*8*, *22*) and NMR (*10*−*12*, *23*, *24*). As discussed in the Introduction, the isolated domain is inactive, or nearly so, and three explanations have been proposed to explain this result: (1) the isolated RNase H domain adopts a significantly different

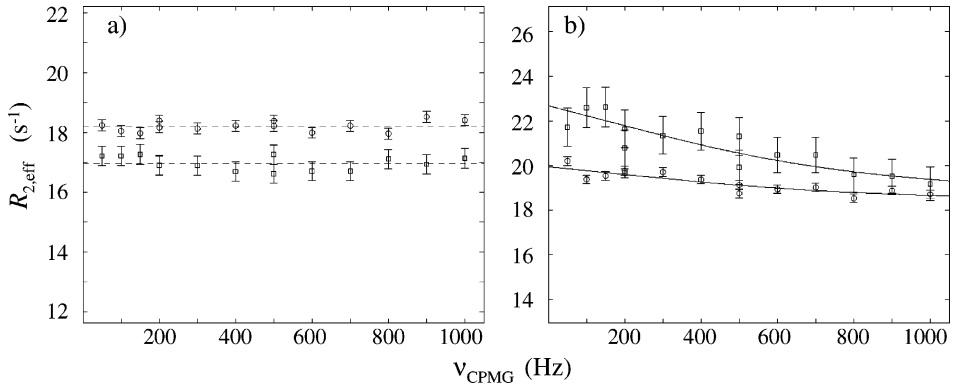

FIGURE 4: Examples of the relaxation dispersion data. The dependence of the intensity of the signal versus CPMG field strength (ν_{CPMG}) for residues Glu92 (a) and Thr48 (b) in the 80 mM Mg-only solution is presented. The data at 11.7 T are indicated with circles, and the data at 18.8 T are indicated with squares. These examples illustrate the best fit to the equations in Tollinger et al. (*31*) corresponding to no detectable exchange (a) and fast exchange (b).

Table 3: R_{ex} Values Derived from CPMG Experiments[a]

residue	SS	low pH τ_{ex} (ms)	Mg only τ_{ex} (ms)	Mg + AMP τ_{ex} (ms)
5				0.34
12				0.71
13			0.19	
15			0.56	
27			0.51	
28				0.06
31	β2		0.11	
34	β2		0.11	0.16
35	β2	0.22	0.47	
38				0.27
42	β3	0.84	7.53	0.32
44	β3			
45	β3			0.62
48	β3	0.21	0.25	0.29
55	αA			0.94
56	αA	0.56		
57	αA	0.42	0.39	
59	αA	0.47		
60	αA		0.06	1.21
67		0.40		
68			0.05	0.06
70	β4			0.61
82	αB		0.06	0.24
84	αB	0.40		
91				1.35
93				0.28
95		1.00		
102	αD			0.34
108	β5		0.41	0.32
113		1.46		
118		0.98		
119				0.64
120			0.19	0.17
121		1.17		
123	αE			0.12
138			0.35	0.34

Slow motions of the RNase H domain were investigated using relaxation dispersion methods. For each residue that was adequately resolved and for which there was adequate signal-to-noise, the results are presented under both solution conditions. The time constants (τ_{ex}) are in ms. The secondary structure is noted next to the residue number.

structure than it does when it is part of the full RT molecule; (2) inactivity of the isolated domain results from pathologically extreme intramolecular dynamic behavior; (3) the isolated domain does not bind to the RNA−DNA hybrid substrate with sufficient affinity to support activity. In general, these explanations need not be mutually exclusive. In addition to the fundamental questions raised by these hypotheses, an evaluation of their relative merits is central to the determination of whether the isolated domain can be used for inhibitor development, since it is much more complex to analyze effects in the full RT molecule.

Relation to Previous NMR Dynamics Characterization. The solution conditions studied here were initially designed to study the response of the enzyme to Mg ions and to AMP at neutral pH. The Mg^{2+} binding affinity of the isolated RNase H domain is very low (*10*). While the Mg^{2+} concentration used in the present studies is much greater than the physiological levels, the high concentration has been introduced to compensate for the absence of substrate, which would provide additional metal ion ligands and hence stabilize the ion-complexed structure. Because the results of these studies were so different from previous results, we repeated the measurements using the solution conditions (pH 5.4) that had been described previously ("low pH").

Previous NMR relaxation studies of the RNase H domain from HIV-1 RT concluded that it is an extremely dynamic entity (*12*). This extreme intramolecular dynamic behavior is evident from the order parameters summarized in Figure 2b (*12*). The most highly mobile regions were identified as the C-terminal residues and the loop regions between β-strands β_1 and β_2 and between α-helix α_B and β_4. Mandel et al. subsequently studied the dynamic behavior of *E. coli* RNase HI and found that this enzyme is characterized by a much narrower range of order parameters than the RNase H domain of RT (*14*, *42*). On the basis of these comparisons, they concluded that the increase in dynamic mobility compared to *E. coli* RNase HI was critical to the lack of catalytic activity of RT RNase H domain (*14*). However, as is apparent from Figure 2a, the dynamic behavior of the RNase H domain studied under a variety of conditions is substantially more homogeneous than the previously reported behavior, with the primary exception of the C-terminal segment, which remains highly mobile. In general, the addition of $MgCl_2$ and AMP increases the $\{^1H\}$-^{15}N NOE ratio (Figure 1c), which is indicative of reduced internal flexibility. In fact, with both Mg^{2+} and AMP in the solution, the numbers of residues that fit to different motional models are similar to the catalytically active *E. coli* RNase H (*14*) (see Table 1). However, it should be noted that the C-terminal helix, α_E, is observable in NMR studies of the *E. coli* RNase HI, while it is subject to severe exchange broadening in the HIV RT RNase H domain, indicating slow conformational

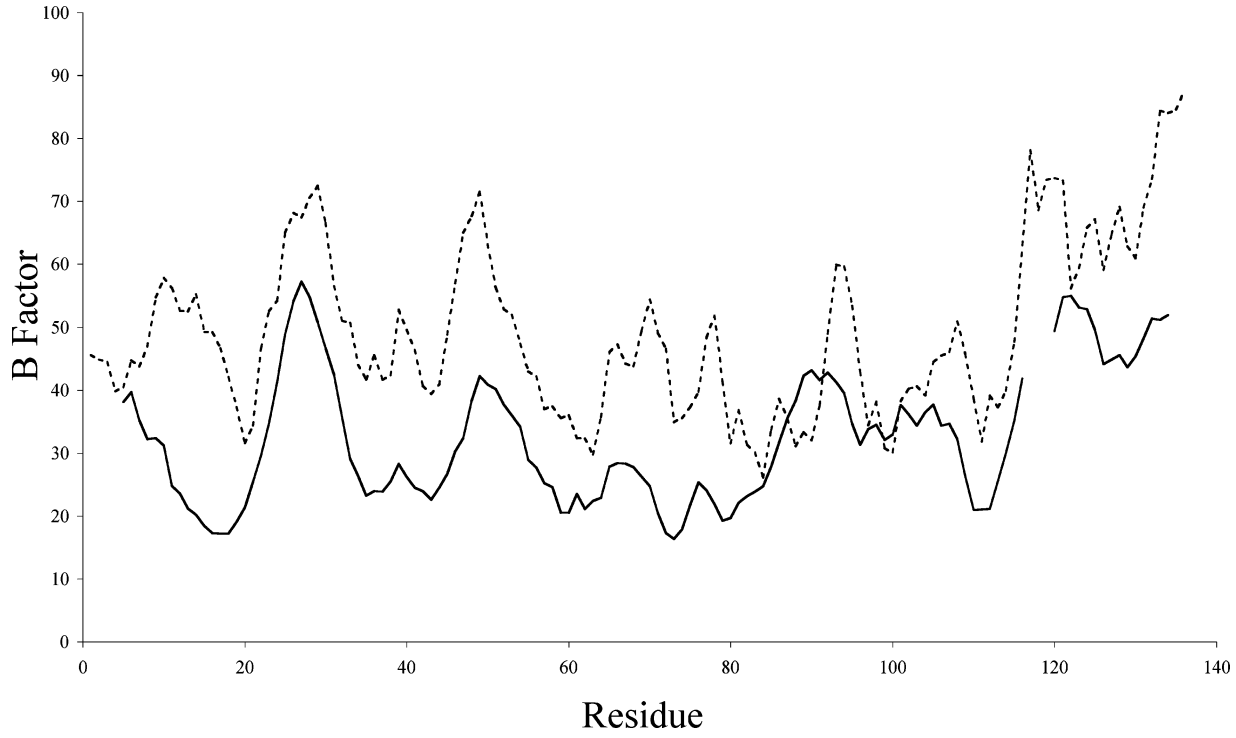

FIGURE 5: Average B-factors in RNase H. The average B-factors of the nitrogen backbone atoms are presented for the isolated domain (solid line) and the domain as part of RT (dashed line) for each residue. For details, see Materials and Methods.

exchange between two or more states. Since this helix (α_E) can be observed in some of the crystal structures of RT, we conclude that at least one of these states contains this structure, while in the remaining state(s) the helix may move or unwind.

The substantial difference in dynamic characterizations illustrated in Figure 2 is most likely the result of substantial improvements in relaxation methodology and order parameter determination methodology that have been made during the past decade (*14*, *19*). It also is worth noting that the very low order parameters plotted previously (*14*) and reproduced in Figure 2b are almost always S^2_f. They are derived from model 5, which was selected 32 times (Table 1), or a hybrid of model 4 and 5, which was fit 12 times. The hybrid model is not currently used and was actually underdetermined based on the data. The overall S^2 is the product of S^2_f and S^2_s, which, if plotted, would make the graph appear somewhat less disjointed. An attempt was made to refit the previous relaxation data with more recently developed analysis techniques (data not shown). In general, we selected less complicated motional descriptions, but much of the data were difficult to fit, i.e., there was a large residual for all models. The differences between the two studies are likely to be a combined effect of improved pulse sequence methodology and analysis.

As shown in the present study, the dynamic behavior of the isolated RT RNase H domain is considerably more uniform than was the case in the previous study; however, the C-terminal region of the protein remains highly dynamic. In addition to the slow dynamic behavior leading to broadening of the resonances of residues in α_E, CPMG experiments indicate that a number of residues in the N-terminal β-sheet are also subject to slow dynamic processes. This could be the result of a slow opening and closing of the β-sheet. However, as can be seen from Figure 3, the C-terminal helix rests against the β-sheet formed from the three N-terminal β-strands. Hence, these β-sheet residues will necessarily experience the slow-time-scale dynamic motion of the adjacent helix. Consistent with this interpretation, the amide groups of residues for which the side chains interact directly with the helix show this selective dynamic effect. This result illustrates an important characteristic of dynamic characterization by NMR spectroscopy, i.e., time-dependent changes in the magnetic environment of particular nuclei will show up as slow (micro-millisecond) dynamic behavior, even if the corresponding residues are immobile. Thus, the slow dynamic characteristics of the N-terminal β-sheet of the RNase H domain probably indicate primarily motion of the adjacent helix rather than motion of the β-sheet itself.

Relation to Crystallographic Data. It is reasonable to hypothesize that some of the enhanced dynamic behavior of the isolated RNase H domain is a consequence of the absence of stabilizing interactions that would be present in the full RT heterodimer. For example, the loop located between helices α_B and α_D exhibits a significant increase in the R_1 relaxation rate (Figure 1) and a decrease in the values of S^2 derived from the model-free analysis (Figure 2). In the full RT molecule, these residues interact with the other residues in the p66 subunit. However, in analyzing the results of order parameter predictions based on a contact model (*36*), this loop is predicted to be dynamic even in the RT structure (data not shown). The loops adjacent to the C terminal helix were also predicted to be highly dynamic, although the active-site loop (residues 116 to 120) makes contact with the P51 subunit in the full RT molecule. Similarly, an examination of the RT structures in the protein database indicates that there are no obvious structural interactions in RT that would be expected to stabilize the C-terminal helix of the RNase H domain. As discussed previously, the variability in the appearance of the C-terminal helix in the

ensemble of reported RT crystal structures also suggests that helix α_E has marginal stability in the full RT molecule (*10*).

A comparison of the crystallographic B-factors determined for the isolated RNase H domain (*8*, *22*) with those reported for this domain in a set of RT crystal structures (*32*−*35*) also provides insight into the effects of the full enzyme on the behavior of the RNase H domain. As shown in Figure 5, the average B-factors for the isolated RNase H domain show trends similar to the average B-factors from the corresponding region of structures of the full RT molecules, although the curves are displaced. The correlation coefficient between the two curves is 0.69, showing reasonably good correlation. Although B-factor analysis cannot separate static disorder from dynamic fluctuation, this comparison provides further support for the conclusion that the dynamic characteristics of the RNase H domain are relatively unaffected by the remainder of the RT structure. Finally, we note that the highest B-factors are generally observed approximately after residue 115, which suggests more mobility, as reflected in the NMR order parameters for this region. Thus, multiple conformations of the C-terminal helix are observed in the isolated domain as well as in the RT molecule, and the isolated domain has dynamic characteristics in the crystalline state that are similar to the domain as part of HIV-1 RT.

In summary, NMR relaxation studies of the RNase H domain indicate considerably less dynamic instability than suggested by previous relaxation studies, most probably due to the more limited methodology used in the earlier studies. In general, the dynamic behavior is very similar to that observed for the catalytically active *E. coli* RNase HI, suggesting that extreme dynamic instability is probably not the reason for the inactivity of the isolated RNase H domain. This conclusion is further buttressed by B-factor analysis and other observations on the crystal structures of RT and the isolated RNase H domain, which suggest limited dynamic differences between the isolated and RT-incorporated RNase H domain. Alternatively, recent NMR studies (unpublished) provide additional support for the conclusion that the absence of important substrate binding residues in the isolated RNase H domain explains its inactivity.

ACKNOWLEDGMENT

The authors thank Dr. Oscar Millet (Barcelona Science Park, Spain), Dr. Frans Mulder (Lund University, Sweden), Dr. Andrew Lee (University of North Carolina at Chapel Hill, NC), and Dr. Yuan Chen (City of Hope, CA) for many helpful discussions. Figure 4 was made with PyMOL (http://pymol.sourceforge.net).

SUPPORTING INFORMATION AVAILABLE

Complete tabulations of fitted relaxation data for each of the samples. This material is available free of charge via the Internet at http://pubs.acs.org.

REFERENCES

1. Schatz, O. F. C., Guniger-Leitch, F., and Le Grice, S. F. J. (1989) Point mutations in conserved amino acid residues within the C-terminal domain of HIV-1 reverse transcriptase specifically repress RNase H function, *FEBS Lett. 257*, 311−314.
2. Schatz, O., Mous, J., and Le Grice, S. F. J. (1990) HIV-1 RT-associated ribonuclease H displays both endonuclease and 3′→5′ exonuclease activity, *EMBO J. 9*, 1171−1176.
3. Tisdale, M. S., T.; Larder, B. A.; Moelling, K. (1991) Mutations within the RNase H domain of human immunodeficiency virus type 1 reverse transcriptase abolish virus infectivity, *J. Gen. Virol. 72*, 59−66.
4. Becerra, S. P., Clore, G. M., Gronenborn, A. M., Karlstrom, A. R., Stahl, S. J., Wilson, S. H., and Wingfield, P. T. (1990) Purification and characterization of the RNase H domain of HIV-1 reverse transcriptase expressed in recombinant *Escherichia coli*, *FEBS Lett. 270*, 76−80.
5. Hostomsky, Z. H., Z.; Hudson, G. O.; Moomaw, E. W.; Nodes, B. R. (1991) Reconstitution in vitro of RNase H activity by using purified N-terminal and C-terminal domains of human immunodeficiency virus type 1 reverse transcriptase, *Proc. Natl. Acad. Sci. U.S.A. 88*, 1148−1152.
6. Stammers, D. K., and Skinner, R. H. (1991) Rapid purification and characterisation of HIV-1 reverse transcriptase and RNaseH engineered to incorporate a C-terminal tripeptide alpha-tubulin epitope: Use of the Glu-Glu-Phe C-terminal epitope for rapid purification of the catalytic domain of normal and mutant ras GTPase-activating proteins, *FEBS Lett. 283*, 298−302.
7. Evans, D. B., Brawn, K., Deibel, M. R., Jr., Tarpley, W. G., and Sharma, S. K. (1991) A recombinant ribonuclease H domain of HIV-1 reverse transcriptase that is enzymatically active, *J. Biol. Chem. 266*, 20583−20585.
8. Davies, J. F., II, Hostomska, Z., Hostomsky, Z., Jordan, S. R., and Matthews, D. A. (1991) Crystal structure of the ribonuclease H domain of HIV-1 reverse transcriptase, *Science 252*, 88−95.
9. Stahl, S. J., Kaufman, J. D., Vikic-Topic, S., Crouch, R. J., and Wingfield, P. T. (1994) Construction of an enzymatically active ribonuclease H domain of human immunodeficiency virus type 1 reverse transcriptase, *Protein Eng. 7*, 1103−1108.
10. Pari, K., Mueller, G. A., DeRose, E. F., Kirby, T. W., and London, R. E. (2003) Solution structure of the RNase H domain of the HIV-1 reverse transcriptase in the presence of magnesium, *Biochemistry 42*, 639−650.
11. Kern, G., Pelton, J., Marqusee, S., and Kern, D. (2002) Structural properties of the histidine-containing loop in HIV-1 RNase H, *Biophys. Chem. 96*, 285−291.
12. Powers, R., Clore, G. M., Stahl, S. J., Wingfield, P. T., and Gronenborn, A. (1992) Analysis of the backbone dynamics of the ribonuclease H domain of the human immunodeficiency virus reverse transcriptase using ^{15}N relaxation measurements, *Biochemistry 31*, 9150−9157.
13. Lipari, G., and Szabo, A. (1981) Model-free approach to the interpretation of nuclear magnetic resonance relaxation in macromolecules. 1. Theory and range of validity, *J. Am. Chem. Soc. 104*, 4546−4559.
14. Mandel, A. M., Akke, M., and Palmer, A. G., 3rd. (1995) Backbone dynamics of *Escherichia coli* ribonuclease HI: correlations with structure and function in an active enzyme, *J. Mol. Biol. 246*, 144−163.
15. Loria, J. P., Rance, M., and Palmer, A. G., III. (1999) A Relaxation-compensated Carr−Purcell−Meiboom−Gill sequence for characterizing chemical exchange by NMR spectroscopy, *J. Am. Chem. Soc. 121*, 2331−2332.
16. Grzesiek, S., and Bax, A. (1993) The importance of not saturating H_2O in protein NMR−Application to sensitivity enhancement and NOE measurements, *J. Am. Chem. Soc. 115*, 12593−12594.
17. Kay, L. E., Keifer, P., and Saarinen, T. (1992) Pure absorption gradient enhanced heteronuclear single quantum correlation spectroscopy with improved sensitivity, *J. Am. Chem. Soc. 114*, 10663−10665.
18. Farrow, N. A., Muhandiram, R., Singer, A. U., Pascal, S. M., Kay, C. M., Gish, G., Shoelson, S. E., Pawson, T., Forman-Kay, J. D., and Kay, L. E. (1994) Backbone dynamics of a free and phosphopeptide-complexed Src homology 2 domain studied by ^{15}N NMR relaxation, *Biochemistry, 33*, 5984−6003.
19. D'Auvergne, E. J., and Gooley, P. R. (2003) The use of model selection in the model-free analysis of protein dynamics, *J. Biomol. NMR 25*, 25−39.
20. Allen, S. J. W., Krawczyk, S. H., McGee, L. R., Bischofberger, N., Mulato, A. S., and Cherrignton, J. M. (1996) Inhibition of HIV-1 RNase H activity by nucleotide dimers and monomers, *Antiviral Chem. Chemother. 7*, 37−45.
21. Tan, C. K., Civil, R., Mian, A. M., So, A. G., and Downey, K. M. (1991) Inhibition of the RNase H activity of HIV reverse transcriptase by azidothymidylate, *Biochemistry 30*, 4831−4835.
22. Chattopadhyay, D., Finzel, B. C., Munson, S. H., Evans, D. B., Sharma, S. K., Strakalaitis, N. A., Brunner, D. P., Eckenrode, F.

M., Dauter, Z., Betzel, C., and Einspahr, H. M. (1993) Crystallographic Analyses of Active HIV-1 Ribonuclease H Domain Show Structural Features that Distinguish it from the Inactive Form, *Acta Crystallogr., Sect. D 49*, 423−427.
23. Kern, G., Handel, T., and Marqusee, S. (1998) Characterization of a folding intermediate from HIV-1 ribonuclease H, *Protein Sci. 7*, 2164−2174.
24. Powers, R., Clore, G. M., Bax, A., Garrett, D. S., Stahl, S. J., Wingfield, P. T., and Gronenborn, A. M. (1991) Secondary structure of the ribonuclease H domain of the human immunodeficiency virus reverse transcriptase in solution using three-dimensional double and triple resonance heteronuclear magnetic resonance spectroscopy, *J. Mol. Biol. 221*, 1081−1090.
25. Mulder, F. A., Skrynnikov, N. R., Hon, B., Dahlquist, F. W., and Kay, L. E. (2001) Measurement of slow (micro-ms) time scale dynamics in protein side chains by 15-N relaxation dispersion NMR spectroscopy: application to Asn and Gln residues in a cavity mutant of T4 lysozyme, *J. Am. Chem. Soc. 123*, 967−975.
26. Delaglio, F., Grzesiek, S., Vuister, G. W., Zhu, G., Pfeifer, J., and Bax, A. (1995) NMRPipe: A multidimensional spectral processing system based on UNIX pipes, *J. Biomol. NMR 6*, 277−293.
27. Johnson, B. A., and Blevins, R. A. (1994) NMRVIEW: a computer program for the visualization and analysis of NMR data, *J. Biomol. NMR*, *4*, 603−614.
28. Press, W. H., Flannery, B. P., Teukolsky, S. A., and Vetterling, W. T. (1989) *Numerical Recipes*, Cambridge University Press, Cambridge.
29. Tjandra, N., Feller, S. E., Pastor, R. W., and Bax, A. (1995) Rotational Diffusion Anisotropy of Human Ubiquitin from N-15 NMR Relaxation, *J. Am. Ch. Soc. 117*, 12562−12566.
30. Kroenke, C. D., Loria, J. P., Lee, L. K., Rance, M., and Palmer, A. G. (1998) Longitudinal and transverse $^{1}H-^{15}N$ dipolor/^{15}N chemical shift anisotropy relaxation interference: Unambiguous determination of rotational diffusion tensors and chemical exchange effects in biological macromolecules, *J. Am. Chem. Soc. 120*, 7905−7915.
31. Tollinger, M., Skrynnikov, N. R., Mulder, F. A., Forman-Kay, J. D., and Kay, L. E. (2001) Slow dynamics in folded and unfolded states of an SH3 domain, *J. Am. Chem. Soc. 123*, 11341−11352.
32. Ren, J. S., Esnouf, R., Hopkins, A., Ross, C., Jones, Y., Stammers, D., and Stuart, D. (1995) The structure of HIV-1 reverse transcriptase complexed with 9-chloro- TIBO: Lessons for inhibitor design, *Structure 3*, 915−926.
33. Huang, H., Chopra, R., Verdine, G. L., and Harrison, S. C. (1998) Structure of a covalently trapped catalytic complex of HIV-1reverse transcriptase: Implications for drug resistance, *Science 282*, 1669−1675.
34. Ren, J. S., Esnouf, R., Garman, E., Somers, D., Ross, C., Kirby, I., Keeling, J., Darby, G., Jones, Y., Stuart, D., and Stammers, D. (1995) High-resolution structures of HIV-1 RT from four RT-inhibitor complexes, *Nat. Struct. Biol. 2*, 293−302.
35. Sarafianos, S. G., Das, K., Ding, J., Boyer, P. L., Hughes, S. H., and Arnold, E. (1999) Touching the heart of HIV-1 drug resistance: The fingers close down on the dNTP at the polymerase active site, *Chem. Biol. 6*, R137−R146.
36. Zhang, F., and Brushweiler, R. (2002) Contact model for the prediction of NMR N−H order parameters in globular proteins, *J. Am. Chem. Soc. 124*, 12654−12655.
37. Brunger, A. T., Adams, P. D., Clore, G. M., DeLano, W. L., Gros, P., Grosse-Kunstleve, R. W., Jiang, J. S., Kuszewski, J., Nilges, M., Pannu, N. S., Read, R. J., Rice, L. M., Simonson, T., and Warren, G. L. (1998) Crystallography & NMR system: A new software suite for macromolecular structure determination, *Acta Crystallogr., Sect. D 54*, 905−921.
38. Lee, A. L., and Wand, A. J. (1999) Assessing potential bias in the determination of rotational correlation times of proteins by NMR relaxation, *J. Biomol. NMR. 13*, 101−12.
39. Millet, O., Loria, J. P., Kroenke, C. D., Pons, M., and Palmer, A. G., 3rd. (2000) The static magnetic field dependence of chemical exchange linebroadening define the NMR chemical shift time scale, *J. Am. Chem. Soc. 122*, 2867−2877.
40. Kempf, J. G., and Loria, J. P. (2003) Protein dynamics from solution NMR: Theory and applications, *Cell Biochem. Biophys. 37*, 187−211.
41. Sarafianos, S. G., Das, K., Tantillo, C., Clark, A. D., Jr., Ding, J., Whitcomb, J. M., Boyer, P. L., Hughes, S. H., and Arnold, E. (2001) Crystal structure of HIV-1 reverse transcriptase in complex with a polypurine tract RNA:DNA, *Embo. J. 20*, 1449−61.
42. Mandel, A. M., Akke, M., and Palmer, A. G., III. (1996) Dynamics of ribonuclease H: temperature dependence of motions on multiple time scales, *Biochemistry 35*, 16009−23.

BI049555N